NASA/TM—2000-210458

The Effect of Boron on the Low Cycle Fatigue Behavior of Disk Alloy KM4

Timothy Gabb and John Gayda
Glenn Research Center, Cleveland, Ohio

Joseph Sweeney
Gilcrest Electric and Supply Company, Brook Park, Ohio

September 2000

The NASA STI Program Office . . . in Profile

Since its founding, NASA has been dedicated to the advancement of aeronautics and space science. The NASA Scientific and Technical Information (STI) Program Office plays a key part in helping NASA maintain this important role.

The NASA STI Program Office is operated by Langley Research Center, the Lead Center for NASA's scientific and technical information. The NASA STI Program Office provides access to the NASA STI Database, the largest collection of aeronautical and space science STI in the world. The Program Office is also NASA's institutional mechanism for disseminating the results of its research and development activities. These results are published by NASA in the NASA STI Report Series, which includes the following report types:

- TECHNICAL PUBLICATION. Reports of completed research or a major significant phase of research that present the results of NASA programs and include extensive data or theoretical analysis. Includes compilations of significant scientific and technical data and information deemed to be of continuing reference value. NASA's counterpart of peer-reviewed formal professional papers but has less stringent limitations on manuscript length and extent of graphic presentations.

- TECHNICAL MEMORANDUM. Scientific and technical findings that are preliminary or of specialized interest, e.g., quick release reports, working papers, and bibliographies that contain minimal annotation. Does not contain extensive analysis.

- CONTRACTOR REPORT. Scientific and technical findings by NASA-sponsored contractors and grantees.

- CONFERENCE PUBLICATION. Collected papers from scientific and technical conferences, symposia, seminars, or other meetings sponsored or cosponsored by NASA.

- SPECIAL PUBLICATION. Scientific, technical, or historical information from NASA programs, projects, and missions, often concerned with subjects having substantial public interest.

- TECHNICAL TRANSLATION. English-language translations of foreign scientific and technical material pertinent to NASA's mission.

Specialized services that complement the STI Program Office's diverse offerings include creating custom thesauri, building customized data bases, organizing and publishing research results . . . even providing videos.

For more information about the NASA STI Program Office, see the following:

- Access the NASA STI Program Home Page at ***http://www.sti.nasa.gov***

- E-mail your question via the Internet to help@sti.nasa.gov

- Fax your question to the NASA Access Help Desk at (301) 621-0134

- Telephone the NASA Access Help Desk at (301) 621-0390

- Write to:
  NASA Access Help Desk
  NASA Center for AeroSpace Information
  7121 Standard Drive
  Hanover, MD 21076

NASA/TM—2000-210458

The Effect of Boron on the Low Cycle Fatigue Behavior of Disk Alloy KM4

Timothy Gabb and John Gayda
Glenn Research Center, Cleveland, Ohio

Joseph Sweeney
Gilcrest Electric and Supply Company, Brook Park, Ohio

National Aeronautics and
Space Administration

Glenn Research Center

September 2000

Available from

NASA Center for Aerospace Information
7121 Standard Drive
Hanover, MD 21076
Price Code: A03

National Technical Information Service
5285 Port Royal Road
Springfield, VA 22100
Price Code: A03

Available electronically at http://gltrs.grc.nasa.gov/GLTRS

THE EFFECT OF BORON ON THE LOW CYCLE FATIGUE BEHAVIOR OF DISK ALLOY KM4

Timothy Gabb and John Gayda
National Aeronautics and Space Administration
Glenn Research Center
Cleveland, Ohio 44135

Joseph Sweeney
Gilcrest Electric and Supply Company
Brook Park, Ohio 44142

Introduction

The durability of powder metallurgy nickel base superalloys employed as compressor and turbine disks is often limited by low cycle fatigue (LCF) crack initiation and crack growth from highly stressed surface locations (corners, holes, etc.). Crack growth induced by dwells at high stresses during aerospace engine operation can be particularly severe (ref. 1, 2). Supersolvus solution heat treatments can be used to produce coarse grain sizes approaching ASTM 6 for improved resistance to dwell fatigue crack growth (ref. 3). However, the coarse grain sizes reduce yield strength, which can lower LCF initiation life. These high temperature heat treatments also can encourage pores to form. In the advanced General Electric disk superalloy KM4, such pores can initiate fatigue cracks that limit LCF initiation life (ref. 4). Hot isostatic pressing (HIP) during the supersolvus solution heat treatment has been shown to improve LCF initiation life in KM4, as the HIP pressure minimizes formation of the pores (ref. 5). Reduction of boron levels in KM4 has also been shown to increase LCF initiation life after a conventional supersolvus heat treatment, again possibly due to effects on the formation tendencies of these pores (ref. 4, 6, 7). However, the effects of reduced boron levels on microstructure, pore characteristics, and LCF failure modes in KM4 still need to be fully quantified. The objective of this study was to determine the effect of boron level on the microstructure, porosity, LCF behavior, and failure modes of supersolvus heat treated KM4.

Material and Experimental Procedures

The compositions of "low boron" and "high boron" KM4 alloys (ref. 7) are listed in Table 1. The overall compositions were comparable, but "low boron" KM4 had about 50% lower boron and 30% higher carbon than the conventional ("high boron") KM4. The alloys were each produced from powder, which was atomized in argon, hot compacted, extruded, then isothermally forged using the same conditions. The low boron KM4 forging was exclusively first subjected to a homogenization/annealing heat treatment of 2140°F/48 h. Specimen blanks were then machined from each forging. The blanks were supersolvus solution heat treated at 2175°F/1h in a vacuum furnace and cooled at an initial cooling rate of about 120°F/min. and then given a subsequent aging heat treatment at 1425°F/8 h. Conventional LCF specimens were then machined with a uniform cylindrical gage section of 0.25" diameter and 0.75" long. The specimen gage sections were subjected to a final low stress grinding/polishing step which produced an 8 rms finish, with final polishing lines oriented parallel to the specimen centerline.

Low cycle fatigue tests were performed at 1200°F with a total strain range of 0.69% and strain ratio $R_\epsilon = \epsilon_{min}/\epsilon_{max}$ of 0. Tests were initially conducted using a strain-controlled sawtooth waveform at a frequency of 0.33 Hertz for about 29,000 cycles. Specimens which survived this test segment were then cycled with a load-controlled sinusoidal waveform at a frequency of 10 Hertz, which maintained the previously stabilized maximum and minimum cyclic stresses. Tests were continued until failure or to a 50% reduction in the maximum stabilized stress. All fracture surfaces were examined using optical and scanning electron microscopy. Planar sections oriented transverse to the specimen centerlines were metallographically prepared adjacent to the fracture surfaces of all specimens, for examination using optical and scanning electron microscopy (SEM). Analyses for pore contents and sizes were performed on the unetched metallographic sections using optical imaging with a Quantimet 500 image analysis system. Grain sizes were determined on the sections after etching with Kallings reagent, using the Heine intercept technique with a circular template according to ASTM E112.

Results and Discussion

1. Typical Microstructures

The low and high boron KM4 alloys had generally similar microstructures after heat treatment. Typical microstructures observed in low and high boron KM4 are compared in Fig. 1. Low boron KM4 specimens had slightly coarser mean grain size (ASTM 5.2±.2) than high boron KM4 (ASTM5.8±.1), but both had mean grain sizes between ASTM 5 and 6. The mean cooling γ' sizes of both alloys were comparably coarse at 0.35-0.38 μm, due to the relatively slow initial cooling rate of about 120F/min. from the solution heat treatment. The low boron KM4 appeared to have a lower pore content than high boron KM4. The characteristics of the pores in each alloy will be subsequently compared in detail.

2. Fatigue Behavior

The KM4 alloys had similar cyclic stress-strain responses. The fatigue test results are listed in Table 2. Cyclic stress-strain hysteresis responses of low and high boron KM4 are compared in Fig. 2. Both alloys had initial plastic strain of over 0.2% on cycle 1, which allowed the determination of 0.2% offset yield strengths on all specimens as indicated on the hysteresis loops of Fig. 2a-b. The yield strengths were quite comparable for all specimens, Fig. 2c. The hysteresis loops in subsequent cycling was predominantly elastic in all specimens, with plastic srain ranges of less than 0.02%. Very little relaxation of cyclic mean and maximum stresses occurred during these tests, and these stresses were maintained near initial levels. The cyclic maximum stress at half of cyclic life of low boron KM4 was slightly higher than that of high boron KM4, Fig. 2c. However, the cyclic stress-strain responses of low and high boron KM4 were very similar overall.

The mean fatigue life of low boron KM4 exceeded that of high boron KM4. The fatigue lives of low and high boron KM4 are compared in the probability diagram of Fig. 3 as the common logarithm of fatigue life versus probability of failure. The data for each alloy should lie along a straight line in this plot, if the common logarithm of life were normally distributed about the mean. Regression lines assuming log normal distributions were fit for each alloy and are shown in the plot. The high correlation coefficients (r^2) of .95 and .88 for low and high boron KM4 indicated the log normal life assumption was reasonable for this data. The mean life (N_f) of each alloy is indicated at a probability of 50%. The regressed mean life of low boron KM4 was 74,085 cycles, significantly longer than that determined for high boron KM4, 21,108 cycles. Mean life of low boron KM4 was longer than that of high boron KM4 at a statistical significance confidence of 99%, using the log normality assumption. As an alternative to the assumption of log normal life, Weibull curves were fit according to the equation:

$$\text{Prob.} = 1 - \exp(-N_f/b)^c$$

The regressed Weibull curves indicated mean lives of 77,268 for low boron KM4 and 24,063 cycles for high boron KM4, similar to previous predictions.

Surface-initiated failures produced lowest lives in both alloys and these failures significantly influenced the life distributions, especially for high boron KM4. Separate life lines are sometimes generated for surface and internal initiated failures (ref. 1). There was an insufficient number of surface-initiated failures to do that in this data set. However, a life comparison excluding surface-initiated failures still indicated low boron KM4 had over 100% longer mean life. Therefore, low boron KM4 conclusively had longer life than high boron KM4 in these test conditions, using either life analysis approach.

3. Evaluation of Failure Initiation Sites

Low and high boron KM4 LCF specimens had different failure initiation sites. The identity, size, and distance from the specimen surface of the observed failure initiation sites in all specimens are listed in Table 3. Typical initiation sites are compared in Fig. 4. Fatigue cracks initiated in low boron KM4 specimens at large grains (facets) and at small, round pores. The small, round pores shall be referred to as Type A pores. However, most failures initiated in high boron KM4 at large, elongated pores, which shall be referred to as Type B pores. The Type B pores were usually at grain boundaries, and sometimes contained minor amounts of agglomerated aluminum and silicon-rich oxide inclusions. Therefore, the

different life responses of low and high boron KM4 could be attributed to different failure initiation sites. The observations indicated the inferior mean life of low boron KM4 was associated with fatigue cracking at large, elongated Type B pores.

4. Evaluation of Life-limiting Features

Pores

Fatigue failures in both low and high boron KM4 often initiated at pores. Therefore, detailed characterizations of pore content and size were conducted in the two alloys. High boron KM4 had higher pore content than low boron KM4. Typical micrographs from metallographic sections of low and high boron KM4 specimens are shown in Fig. 5. Area fractions of porosity were measured by image analyses on a metallographic section from the gage of all tested specimens, and these are compared in Fig. 6. High boron KM4 specimens clearly had higher porosity content than low boron KM4 specimens. Standard deviations in area fractions measured in multiple fields within each section and across all specimens indicated high boron KM4 had a higher area fraction of porosity than low boron KM4 at a statistical confidence level of over 99.9%.

Pore size distributions were also measured in all specimens. The shape of the overall pore size distributions of the two alloys were similar. The pore size distributions of typical low boron and high boron KM4 specimens are compared in Fig. 7. Pore size is expressed here as the diameter of a circle having the equivalent area to the pore (equivalent circle diameter). The higher porosity content of high boron KM4 is clearly evident, with roughly 100% higher numbers of pores detected for each pore size range. The pore size distributions were generally similar, with increasing frequency for decreasing pore size. The minimum pore size indicated in the distributions was limited by the ultimate resolution possible in low magnification images, rather than the actual minimum pore size. Low magnification images of 50X were employed to insure capturing a large majority of the section area and large pores in each metallographic section. Therefore, smaller pores than indicated were present, but were not resolved.

Additional evaluations were directed at large pores, as the fractographic results had indicated that large pores initiated cracks in both alloys. A comparison of the pore size distributions of Fig. 7 had indicated that the largest pores in the high boron specimen exceeded those in the low boron KM4 specimen. Therefore, the maximum length of the largest pore in each specimen section was determined. Maximum pore lengths were confirmed to be larger in the high boron KM4 specimens. Micrographs of the largest pores in typical low and high boron specimens are compared in Fig. 8. The largest pores in low boron specimens were near-spherical Type A pores with maximum lengths of 19-25 μm. However, the largest pores in high boron specimens were the larger, more elongated Type B pores. The maximum lengths of the largest pores in all specimens are compared in Fig. 9. The maximum lengths of pores which initiated failures are also included for comparison. High boron KM4 clearly had significantly larger pores than low boron KM4, both within typical metallographic sections, and at failure initiation sites. In both alloys, the maximum pore length measurements were larger for pores present at failure initiation sites than in metallographic sections. This suggests that fatigue cracking occurs preferentially at the largest pores present in the entire volume of the gage section, which should generally exceed that measured in these randomly selected metallographic sections.

Additional metallographic evaluations were conducted to determine the origins of the large Type B pores in high boron KM4. These pores usually resided at grain boundaries, and they could originate from borides which often extended from grain boundary triple points in high boron KM4. Optical and scanning electron images of a boride are shown in Fig. 10. An energy dispersive x-ray spectrum (EDS) of this boride is shown in Fig. 11. EDS and selected area diffraction pattern analyses by scanning and transmission electron microscopy indicated these were $(Mo,Cr)_3B_2$ borides. These borides often had small pores within them, and were sometimes attached to the ends of larger pores. It has previously been postulated that these borides may be subject to incipient melting during the solution heat treatment of KM4, due to the lower melting point of the borides than the γ-γ' phases (ref. 4). The formation of the large pores could be associated with this process. However, many of the large Type B pores were observed with no borides attached. No consistent evidence of incipient melting of the γ-γ' phase, as reflected by pores surrounded by eutectic layers, was observed at the borides or the large Type B pores. Therefore,

while the borides may be subject to incipient melting during the solution heat treatment, they did not seem directly responsible for the large Type B pores.

While the specific pore formation mechanism is not clear from these observations, it is clear that the large pores form due to differing processing properties of low and high boron KM4. The two alloys may require different powder atomization, compaction, extrusion, or forging conditions to achieve the same pore content after supersolvus heat treatments. Previous work has shown that the homogenization/annealing heat treatment of 2140°F/48 h applied exclusively to low boron KM4 was not responsible for its lower pore content (ref. 6). This heat treatment appeared to increase pore content in both low and high boron KM4 in that study. Systematic evaluations of the effects of each processing step on final pore content would be necessary to fully understand the origins of the large Type B pores, and their relationships to overall boron content and boron content near the grain boundaries.

Grains

The other microstructural features initiating failures were large grains, Fig. 4a. The grains which initiated failures appeared to be much larger than the mean grain size. Therefore, the maximum length of the largest grain in the metallographic section of each specimen was determined. Low boron KM4 had the largest grains and maximum grain lengths. Typical examples of the largest grains observed in low and high boron KM4 are shown in Fig. 12. The results of measurements of all specimens are compared schematically in Fig. 13. Mean grain sizes of low and high boron KM4 were very similar. However the maximum grain length in low boron KM4 was greater that than in high boron KM4 at a statistical confidence of over 99.9%.

The higher maximum grain length in low boron KM4 would not likely be related to its lower boron content than high boron KM4, or the homogenization/annealing pre-conditioning heat treatment of this alloy. The lower boron content was apparently responsible for a reduced number and size of borides pinning grain boundaries in low boron KM4. However, the number and size of MC carbides pinning grain boundaries were equal or greater in low boron KM4, due to the higher carbon level in this alloy. These MC carbides form at higher temperatures, and are considered more effective at pinning grain boundaries than borides.

More likely, the 2140°F/48 h preconditioning heat treatment applied to low boron KM4 before solution heat treating may have been responsible for the higher maximum grain length. It has been shown in supersolvus heat treated Rene' 88DT that subsolvus preconditioning heat treatments can anneal the microstructure by relieving forging strains retained in the grains and by encouraging recrystallization and growth of smaller, new grains (ref. 8). These responses helped to avoid enhanced localized or critical grain growth (CGG), which is driven by high strain and high strain rate forging deformation. However, the preconditioning heat treatment of 2140°F/48 h applied to low boron KM4 was at a higher temperature near the γ' solvus temperature of KM4, which apparently allowed enhanced growth of selected grains to occur before and during the solution heat treatment. This may have overwhelmed any benefits of annealing and recrystallization for preventing CGG.

The maximum lengths of grain facets initiating failures in low boron KM4 were also measured, with the specimen centerline oriented normal to the viewing axis as for the metallographic sections. These results were previously listed in Table 3, and are compared to the maximum grain lengths from metallographic sections in Fig. 13. The maximum grain facet lengths at failure initiation points in low boron KM4 were slightly smaller than the maximum grain lengths of the metallographic sections. The planar metallographic sections only sampled a very small proportion of the grains in the gage section, and larger grains than those measured in each randomly selected section would certainly be expected elsewhere in the gage section volume. These results indicated the largest grains did not initiate failures in low boron KM4, rather relatively large grains meeting other failure criteria initiated the dominant cracks to produce failure.

Other possible failure criteria promoting the planar failure of relatively large grains could include crystallographic grain orientations allowing high resolved shear stresses on active slip systems and high local stress state due to surface effects and residual stresses. The crystallographic orientation effects on slip within grains do appear significant, as suggested by Fig. 14. The machined side adjoining the grain facet which initiated LCF failure in a low boron KM4 specimen is shown. Slip offsets associated with

bands of concentrated slip can be discerned , parallel to the failure plane of the grain. Such slip steps apparently promoted crack initiation and growth on the slip plane. Therefore, planar "facet" failures of large grains in low boron KM4 appeared to be related to concentrated crystallographic slip. The degree of slip concentration expected in a grain could be dependent on crystallographic orientation for resolved stresses, grain boundary characteristics, and local stress state. The degree of slip concentration expected in a grain could increase with grain size to initiate earlier grain and subsequent specimen failures. Alternatively, grains of varying sizes having high slip concentration due to the other considerations could have similar propensities for planar failures, and the larger initial crack produced by failures of larger grains would produce earlier specimen failures. Such considerations could explain why failures initiated at relatively large grains in low boron KM4.

Surface Defects

Two of the three surface-initiated failures producing lowest lives in the KM4 alloys occurred at scratches. This indicates these surface defects were also important life-limiting features. The shallow scratches of 5-6 μm depth were apparently produced during machining, handling, or test setup of the specimens. Surface-initiated failures at such minor scratches indicate surface finish and surface preparation techniques such as shot peening are important considerations in maximizing the LCF lives of advanced disk alloys such as KM4 (ref. 9). Surface crack initiated LCF failures can be up to 10X lower than internal initiated failures in powder metallurgy disk alloys in similar test conditions (ref. 1). Therefore, machined surfaces are also important potential crack initiation sites which must be understood and controlled in the disk production process.

Summary and Conclusions

In summary, the fatigue behavior and failure mechanisms of low and high boron KM4 powder metallurgy disk superalloys were compared. Low and high boron KM4 alloys had comparable strength and cyclic stress-strain behaviors. However, low boron KM4 had over 100% longer mean life than high boron KM4 for the test conditions employed. The inferior life high boron KM4 specimens had failures initiating mainly at large, elongated Type B pores located at grain boundaries. These large Type B pores could be associated with $(Mo,Cr)_3B_2$ borides or could be due to differing boron-dependent processing requirements for low and high boron KM4. Low boron KM4 lives were mainly limited by cracks initiating at smaller Type A pores and at planar failures of large grains (facets). Single specimens of both alloys also had surface-initiated failures from surface scratches, which produced the lowest lives.

It can be concluded from this study that supersolvus heat treatments employed to produce coarse grain size for improved dwell fatigue crack growth resistance present challenges to LCF initiation resistance:

1) Coarser average grain size produces lower yield strength and increased plastic flow for an alloy, which can lower mean LCF life for a given strain range.
2) Nonuniform grain growth can produce inordinately large grains, which can be crack initiation sites.
3) Large pores can form, which can be crack initiation sites.

Composition adjustments such as those performed here for KM4 can address some of these challenges, however a comprehensive consideration of the entire powder metallurgy disk production process appears necessary to maximize LCF initiation life in supersolvus heat treated disk alloys. The effects on LCF initiation life of alloy composition, powder characteristics, thermomechanical processing, heat treatment, non-destructive evaluation, machining, and final surface preparation techniques such as shot peening all need to be understood.

References

1. D. R. Chang, D. D. Kruger, and R. A. Sprague, "Superalloy Powder Processing, Properties, and Turbine Disk Applications", in Superalloys 1984, TMS-AIME, Warrendale, PA, 1984, pp. 247-273.
2. J. Gayda, T. P. Gabb, and R. V. Miner, "On the Fatigue Crack Propagation Behavior of Superalloys at Intermediate Temperatures", in Superalloys 1984, TMS-AIME, Warrendale, PA, 1984, pp. 733-741.

3. K. R. Bain, M. L. Gambone, J. M. Hyzak, and M. C. Thomas, "Development of Damage Tolerant Microstructures in Udimet 720", in Superalloys 1988, TMS-AIME, Warrendale, PA, 1988, pp. 13-22.
4. E. S. Huron, R. L. Casey, M. F. Henry, and D. P. Mourer, "The Influence of Alloy Chemistry and Powder Production Methods on Porosity in a P/M Nickel-base Superalloy", in Superalloys 1996, ed. by R. D. Kissinger, K. J. Deye, K. L. Anton, A. D. Cetel, M. V. Nathal, T. M. Pollock, and D. A. Woodford, TMS-AIME, 1996, pp. 667-676.
5. J. Gayda and T. P. Gabb, "The Effect of Rapid Quench HIP on the Fatigue Life of the Nickel-Base Superalloy KM4", NASA TM-106717, National Aeronautics and Space Administration, Washington, D.C., 1994.
6. J. Gayda, T. P. Gabb, and M. J. Miller, "Effect of Boron Content on the Fatigue Life of KM4", NASA TM-107166, National Aeronautics and Space Administration, Washington, D.C., 1996.
7. High T3 Disk Alloy Development, Final Report, NASA Contract NAS3-26617, Task Order No. 8, GE Aircraft Engines, 1995.
8. C. P. Blankenship, Jr., M. F. Henry, J. M. Hyzak, R. B. Rohling, and E. L. Hall, "Hot-Die forging of P/M Ni-Base Superalloys", in Superalloys 1996, ed. by R. D. Kissinger, K. J. Deye, K. L. Anton, A. D. Cetel, M. V. Nathal, T. M. Pollock, and D. A. Woodford, TMS-AIME, 1996, pp. 653-662.
9. P. A. Domas, "Elevated Temperature Component Fatigue Robustness-An Holistic Approach", presented at the AGARD Specialist's Meeting, TMF of Aircraft Engine Materials, 1995.

Table 1. Compositions of low and high boron KM4 alloys in weight percent.

Alloy	B	Al	C	Co	Cr	Mo	Nb	Ti	Zr	Ni
Low Boron KM4	0.014	4.1	0.036	18	11.5	3.6	1.9	4	0.037	bal.
High Boron KM4	0.027	4	0.027	18	11.5	3.7	1.9	4	0.04	bal.

Table 2. Fatigue test results.

Alloy	Spec.	Elastic Modulus (Msi)	Strain Range (%)	0.2% Yield Strength σ_y (ksi)	Max. Stress Cycle 1 σ_{max} (ksi)	Min. Stress Cycle 1 σ_{min} (ksi)	Max.Stress at Cycle .5N_f σ_{max} (ksi)	Min. Stress Cycle .5N_f σ_{min} (ksi)	Life N_f (cycles)
Low	.015B-A	26.8	0.7	131.7	131.8	-53	135.7	-46.5	100,422
Boron	.015B-B	26.8	0.7	131.5	132	-52.7	135.5	-47.4	54,462
KM4	.015B-C	27.4	0.7	125	125.7	-56.8	131.7	-51.2	75,410
	.015B-D	27.5	0.7	133.4	134.3	-51.8	134.8	-49.5	67,180
	.015B-E	27.5	0.7	134.7	132.7	-49.6	137	-44.2	54,351
	.015B-F	27.7	0.7	129.7	131	-53.6	133.1	-50	109,796
	MEAN			131.0	131.3	-52.9	134.6	-48.1	
	Stan.Dev.			3.4	2.9	2.4	1.9	2.6	
High	.03B-2	28.3	0.7	130.5	131.1	-60.9	127.5	-65.2	7,510
Boron	.03B-3	28	0.7	131	131.2	-53.7	131.3	-51.5	26,693
KM4	.03B-4	26.4	0.7	129.5	129.2	-51.1	127.7	-55.5	6,265
	.03B-5	27	0.7	130.6	130	-53.8	133.7	-49	28,500
	.03B-6	26.8	0.7	131.4	131.4	-52.8	130.5	-53.3	58,900
	.03B-7	26.4	0.7	130.7	131.2	-55.1	129.5	-55.7	41,952
	MEAN			130.6	130.7	-54.6	130.0	-55.0	
	Stan.Dev.			0.6	0.9	3.4	2.3	5.6	

Table 3. Failure initiation sites in all test specimens, with depth class defined as: I-internal, NS-near surface with minimum defect depth less than maximum defect length, and S-surface.

Alloy	Spec.	Life (cycles)	No. Init.	Identity	Depth Class	Defect Length (mm)	Defect Width (mm)	Min. Depth (mm)	Max. Depth (mm)
Low	.015B-A	100,422	1	A Pore	I	28	17	109	136
Boron	.015B-B	54,462	1	A Pore	I	44	21	106	148
KM4	.015B-C	75,410	1	Facet	I	350	272	743	1037
	.015B-D	67,180	2	Facet	NS	318	123	25	257
				Facet	NS	236	121	11	224
	.015B-E	54,351	2	Scratch	S	19	6	0	6
				A Pore	I	24	19	71	95
	.015B-F	109,796	2	Facet	I	62	14	1683	1733
				A Pore	I	17	12	2554	2566
	MEAN		Facets:			241.5	132.5		
	Stan.Dev.					128.9	106.0		
	MEAN		A Pores:			28.3	17.3		
	Stan.Dev.					11.4	3.9		
High	.03B-2	7,510	1	Scratch	S	40	5	0	5
Boron	.03B-3	26,693	1	B Pore	NS	93	60	34	105
KM4	.03B-4	6,265	1	B Pore	S	61	44	0	44
	.03B-5	28,500	1	B Pore	I	125	75	800	890
	.03B-6	58,900	2	B Pore	I	123	93	2858	2951
				B Pore	I	79	43	2235	2303
	.03B-7	41,952	1	B Pore	I	82	38	508	563
	MEAN		B Pores:			93.8	58.8		
	Stan.Dev.					25.5	21.6		

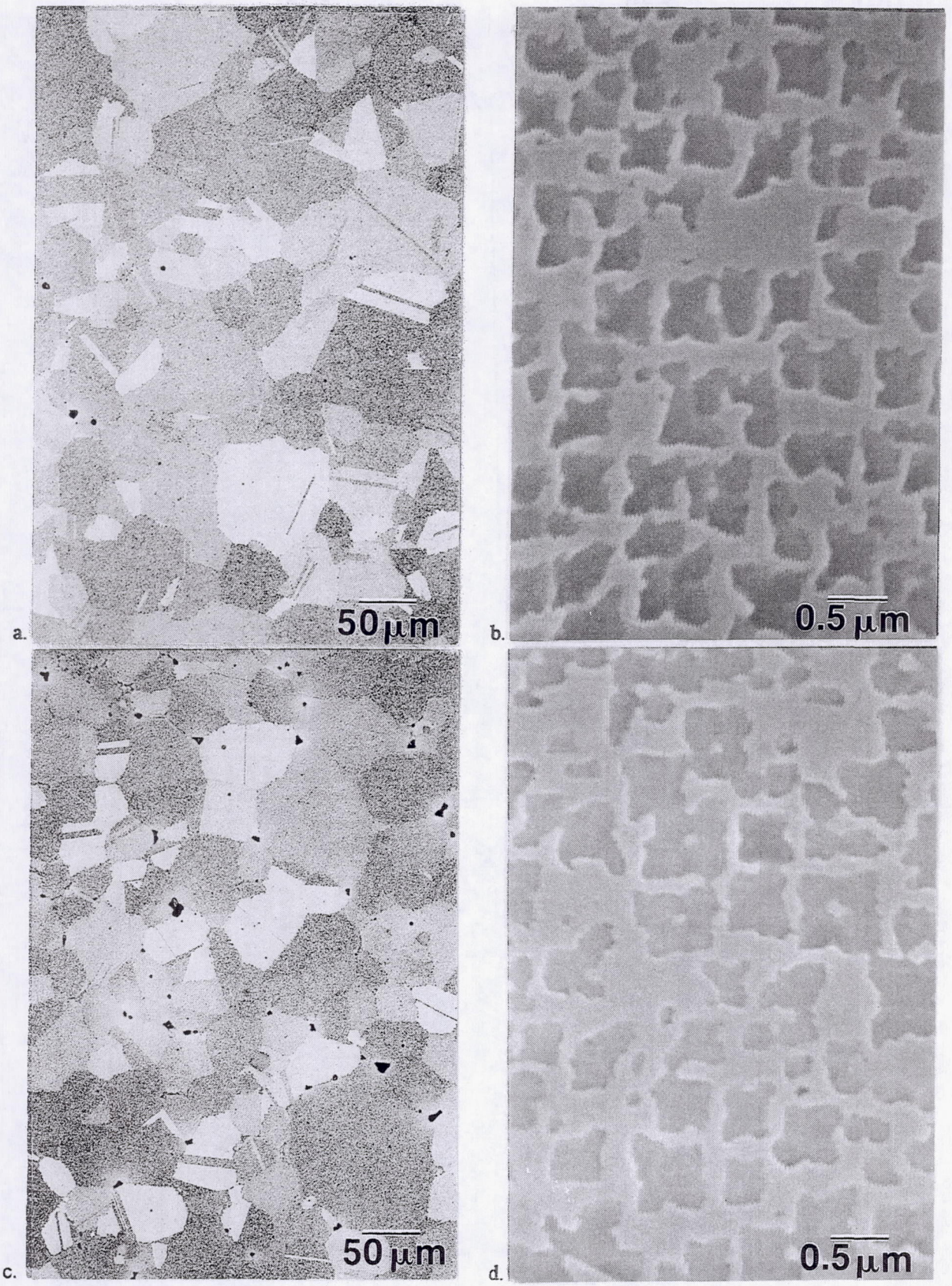

Fig. 1. Typical microstructures: a.-b. low boron KM4, c.-d. high boron KM4.

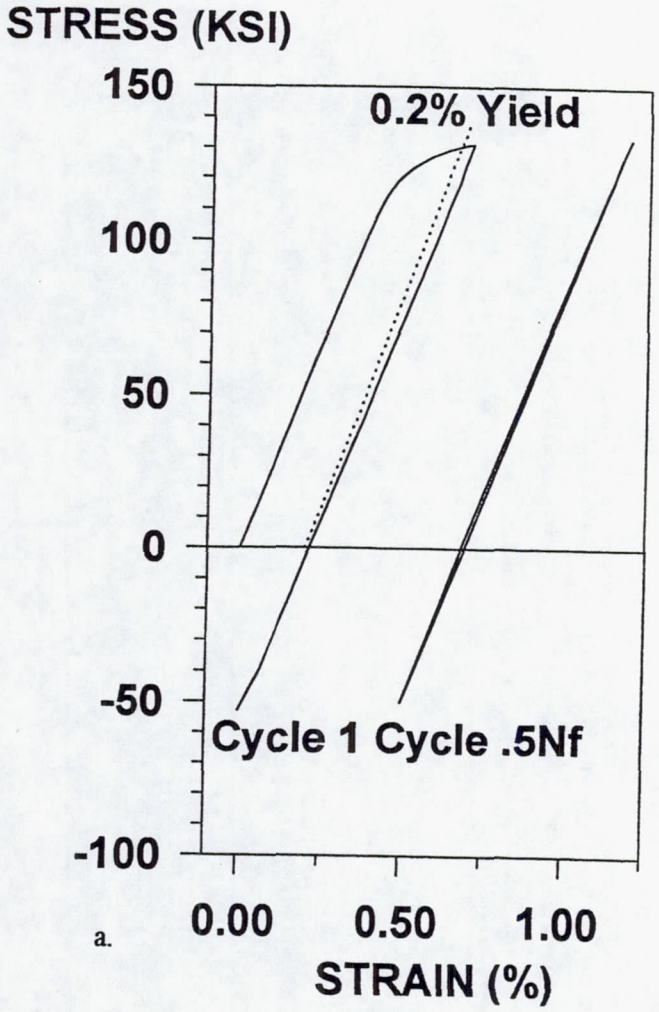

a.

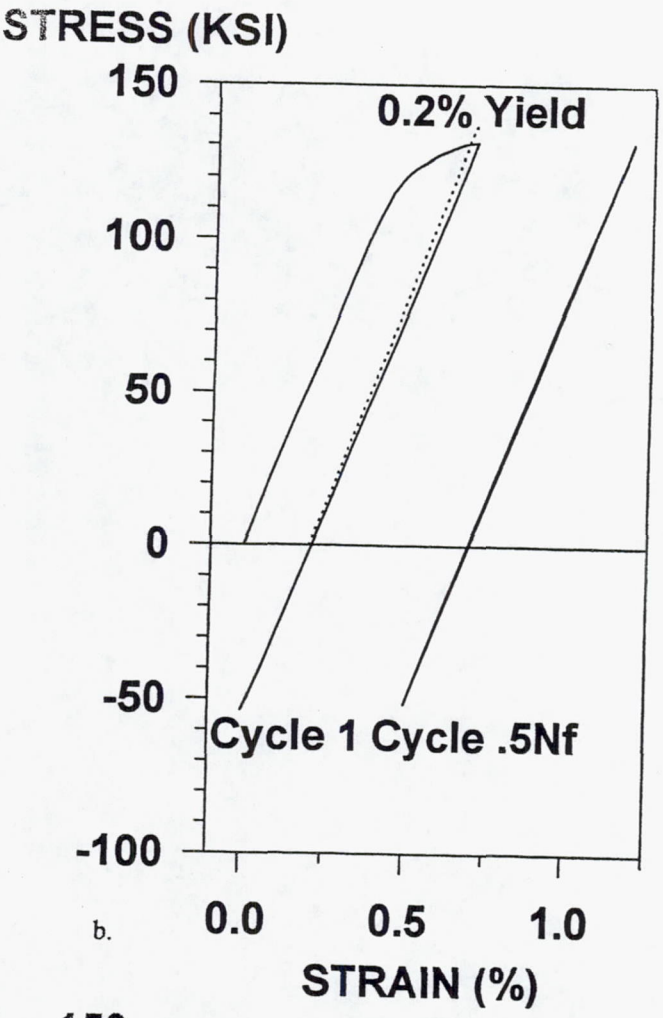

b.

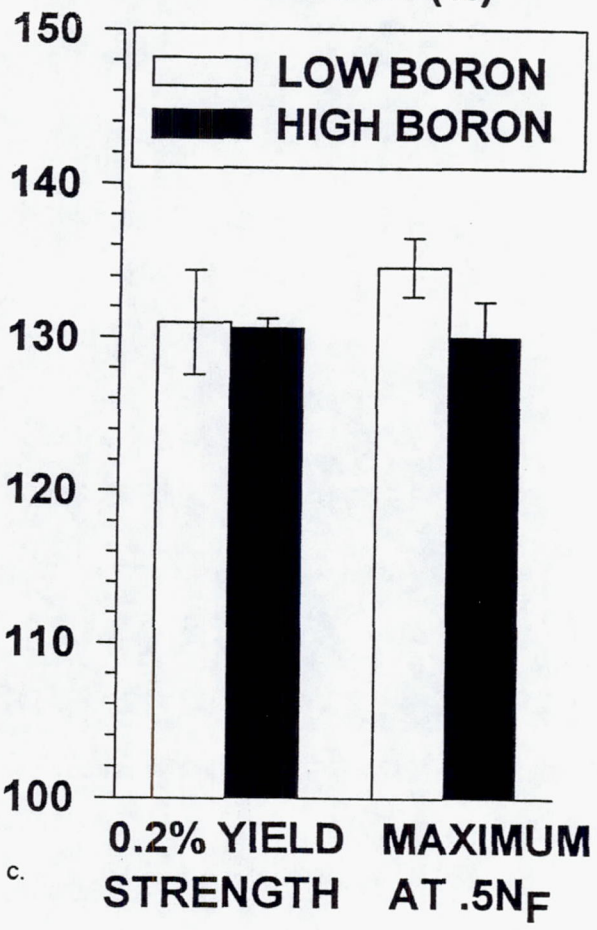

c.

Fig. 2. Typical cyclic stress-strain hysteresis loops: a. low boron KM4, b. high boron KM4, c. comparison of initial yield strength and maximum stress at half of cyclic life for all specimens, error bars indicate ±1 standard deviation.

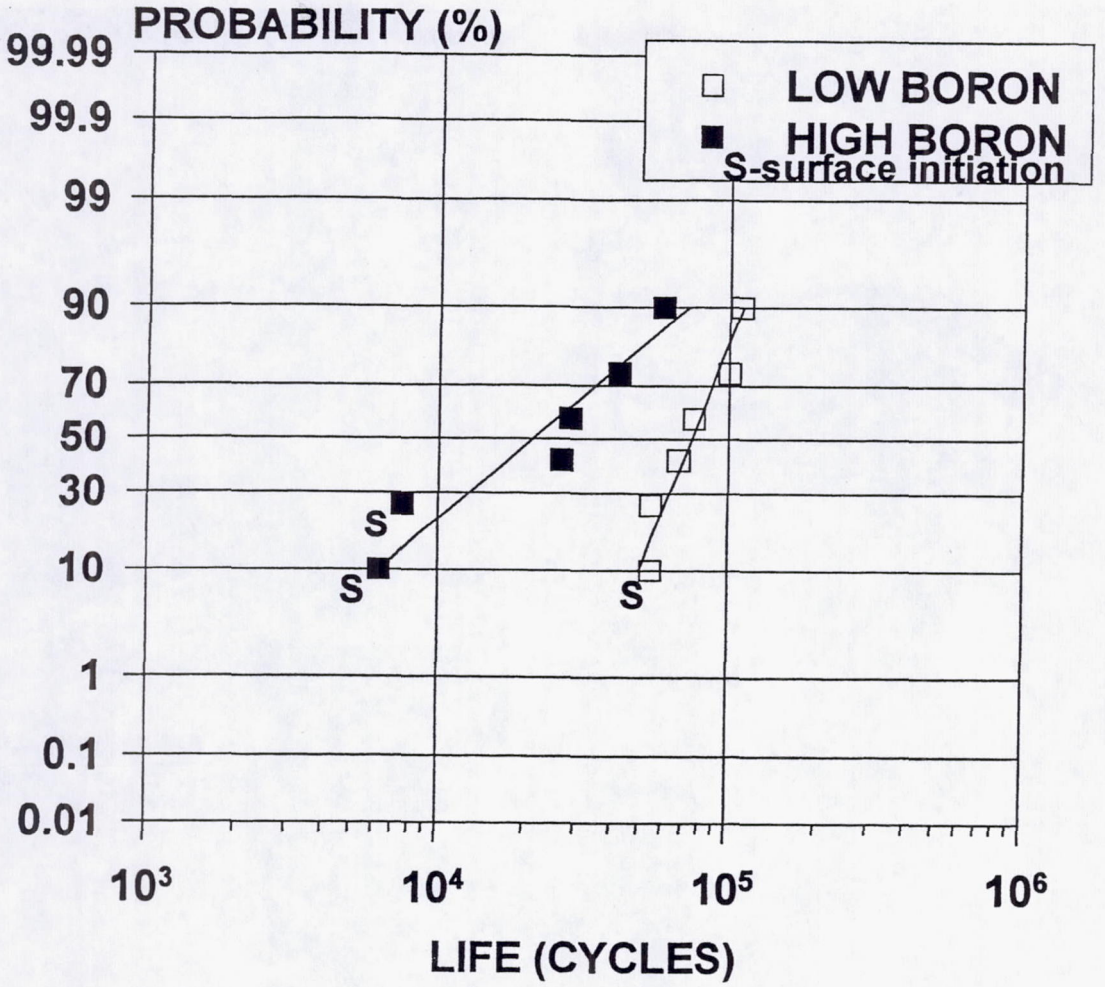

DISTRIBUTION ASSUMPTION	MEAN LIFE (PROB.=50%)	
	LOW B	HIGH B
LOG NORMAL	74,085	21,108
WEIBULL	77,268	24,063

Fig. 3. Probability diagram with comparison of low and high boron KM4 fatigue lives.

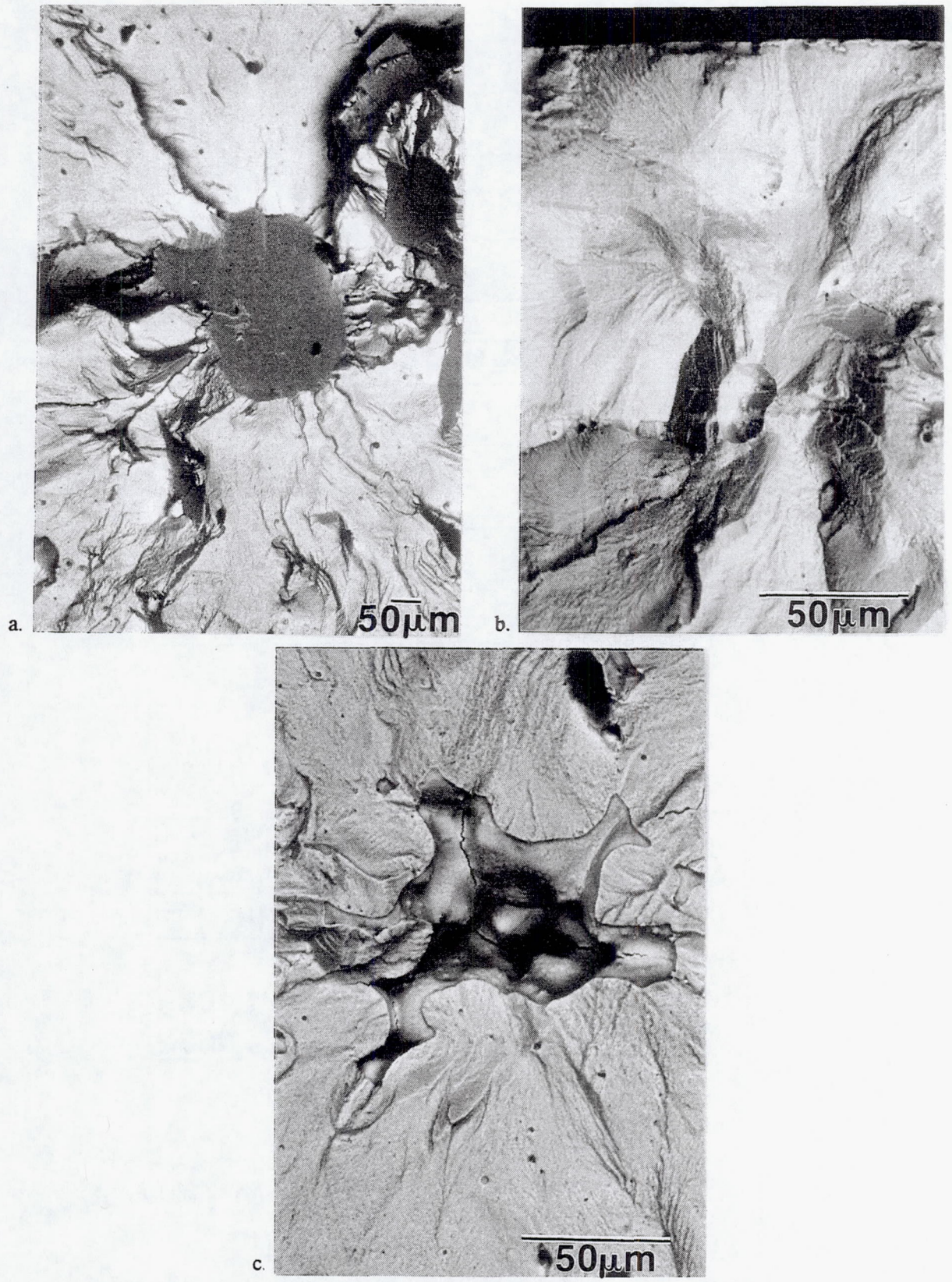

Fig. 4. SEM backscattered electron micrographs of typical failure initiation sites: a. grain facet in low boron KM4, b. small Type A pore in low boron KM4, c. large Type B pore in high boron KM4.

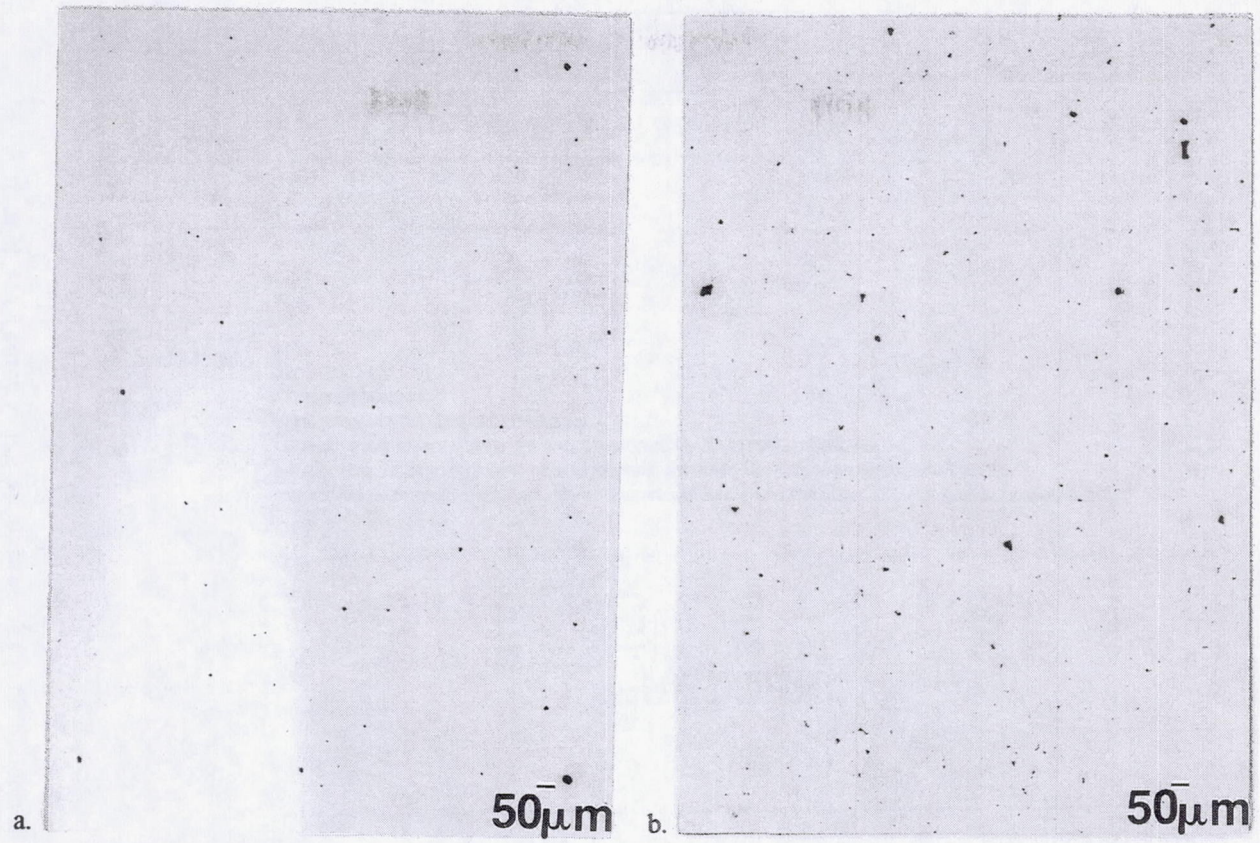

Fig. 5. Optical micrographs showing typical pore content in a. low boron KM4, b. high boron KM4.

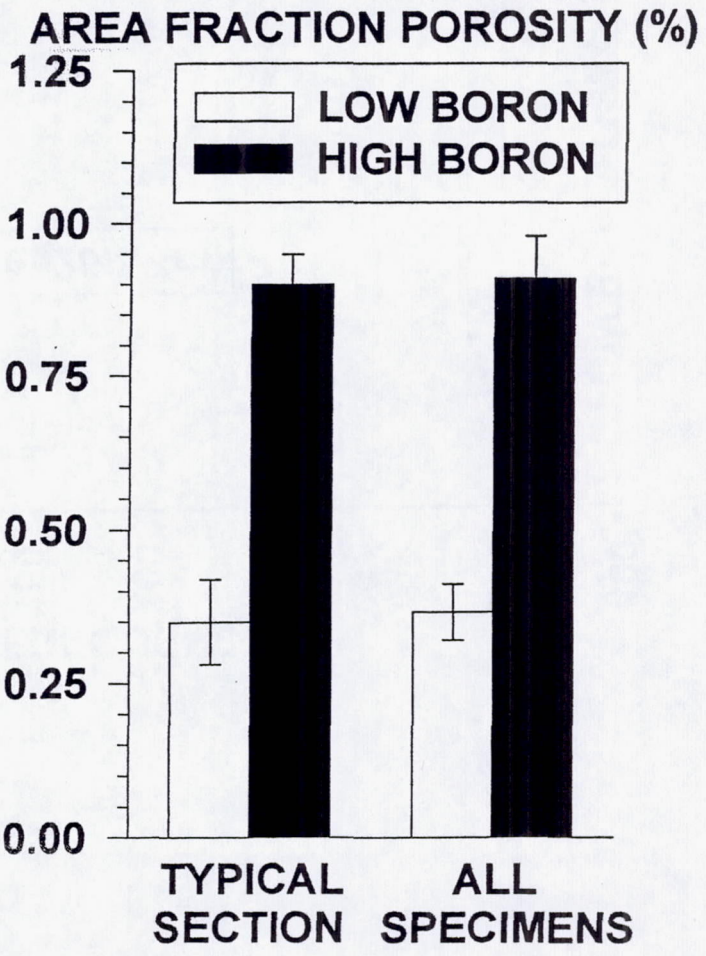

Fig. 6. Comparison of the area fraction of porosity in all specimens, error bars indicate ±1 standard deviation.

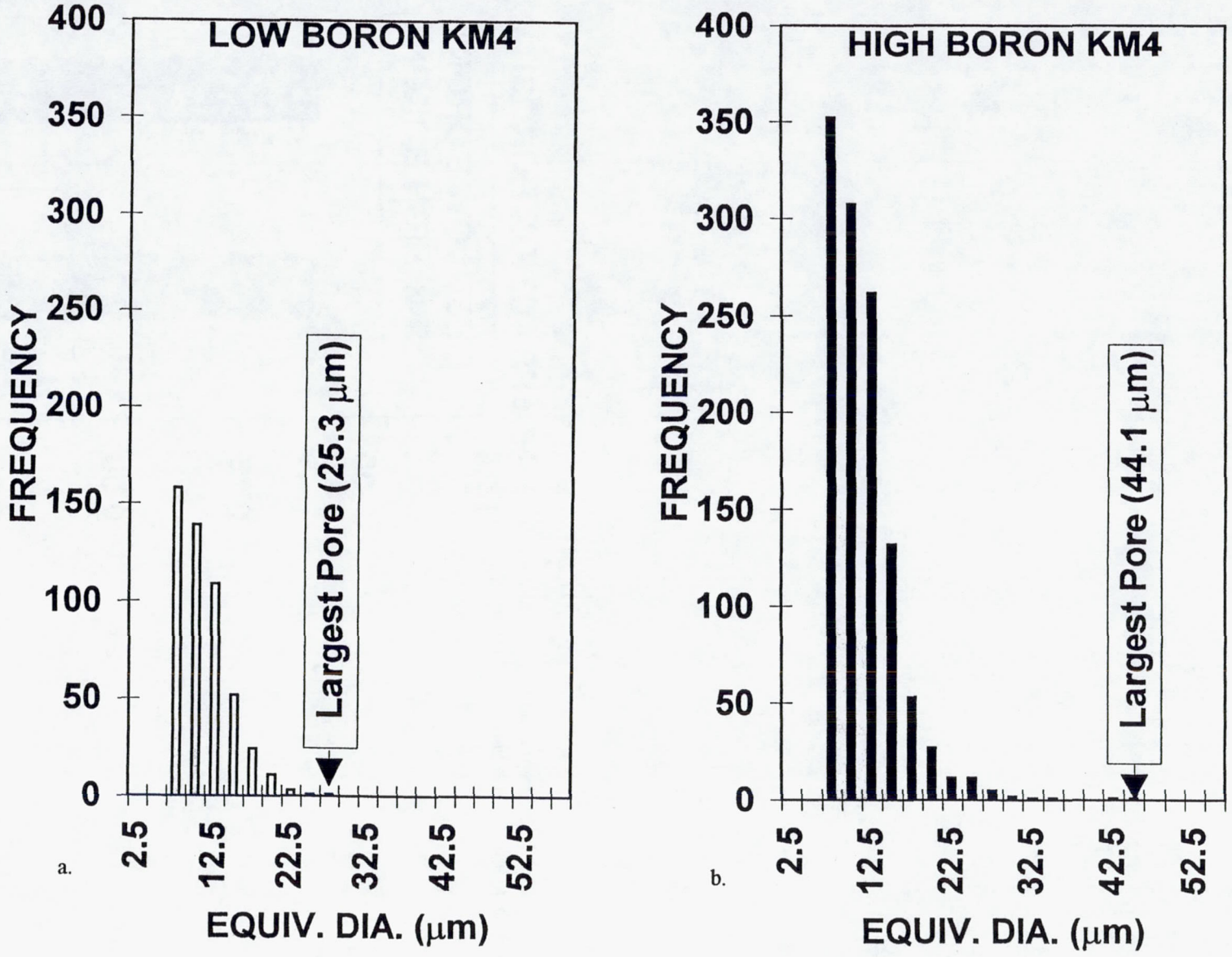

Fig. 7. Typical pore size versus frequency distributions in specimen sections: a. low boron KM4, b. high boron KM4.

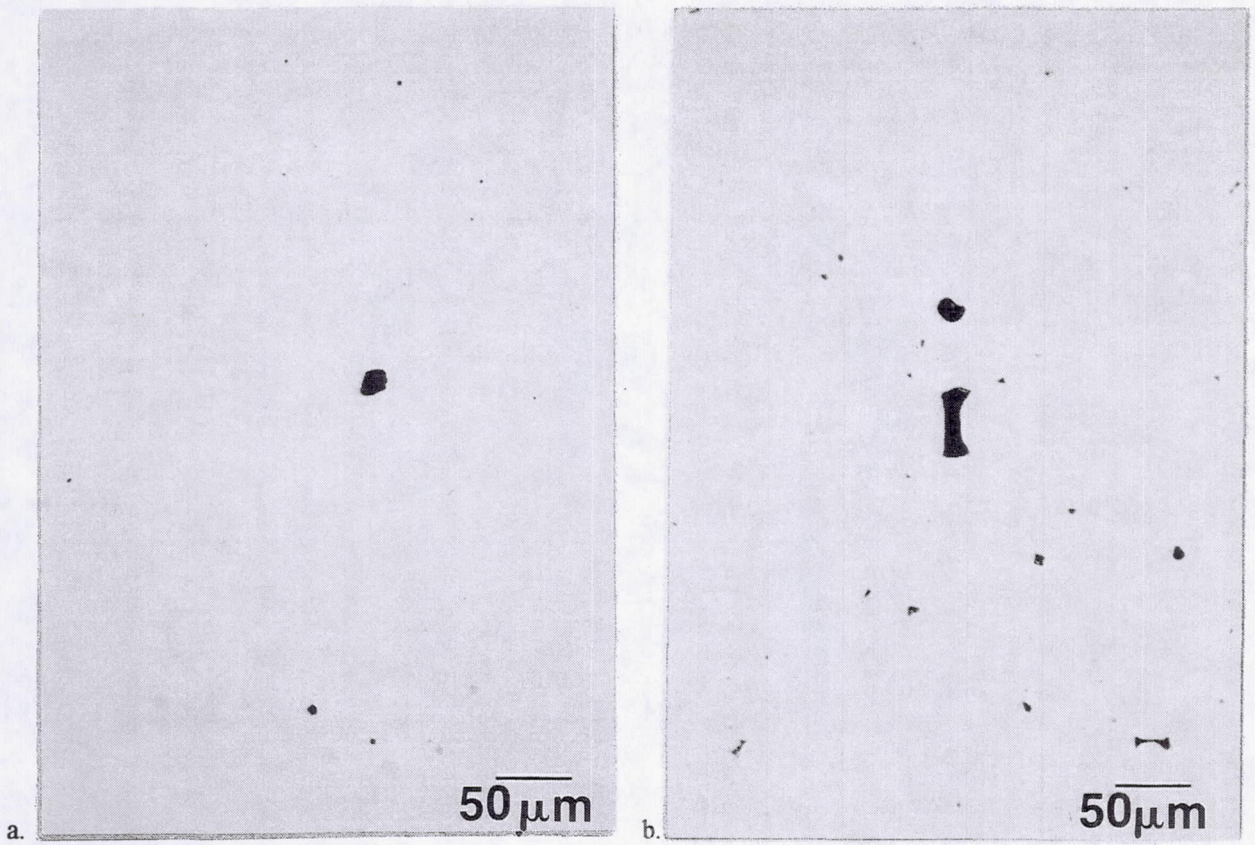

Fig. 8. Optical micrographs showing largest pores in typical specimens: a. low boron KM4, b. high boron KM4.

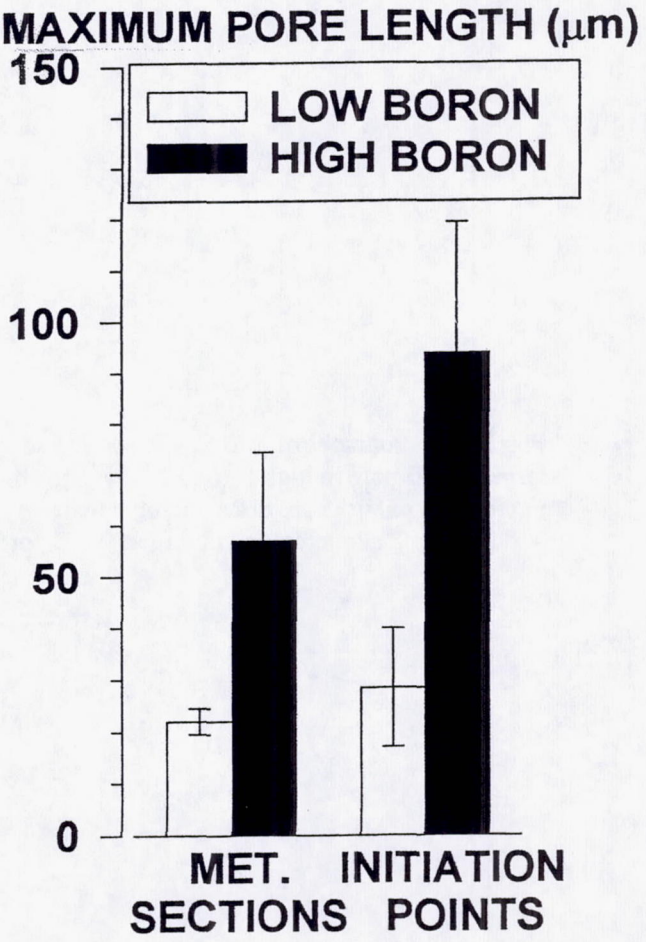

Fig. 9. Comparison of the maximum pore lengths for all specimen sections and at failure initiation sites, error bars indicate ±1 standard deviation.

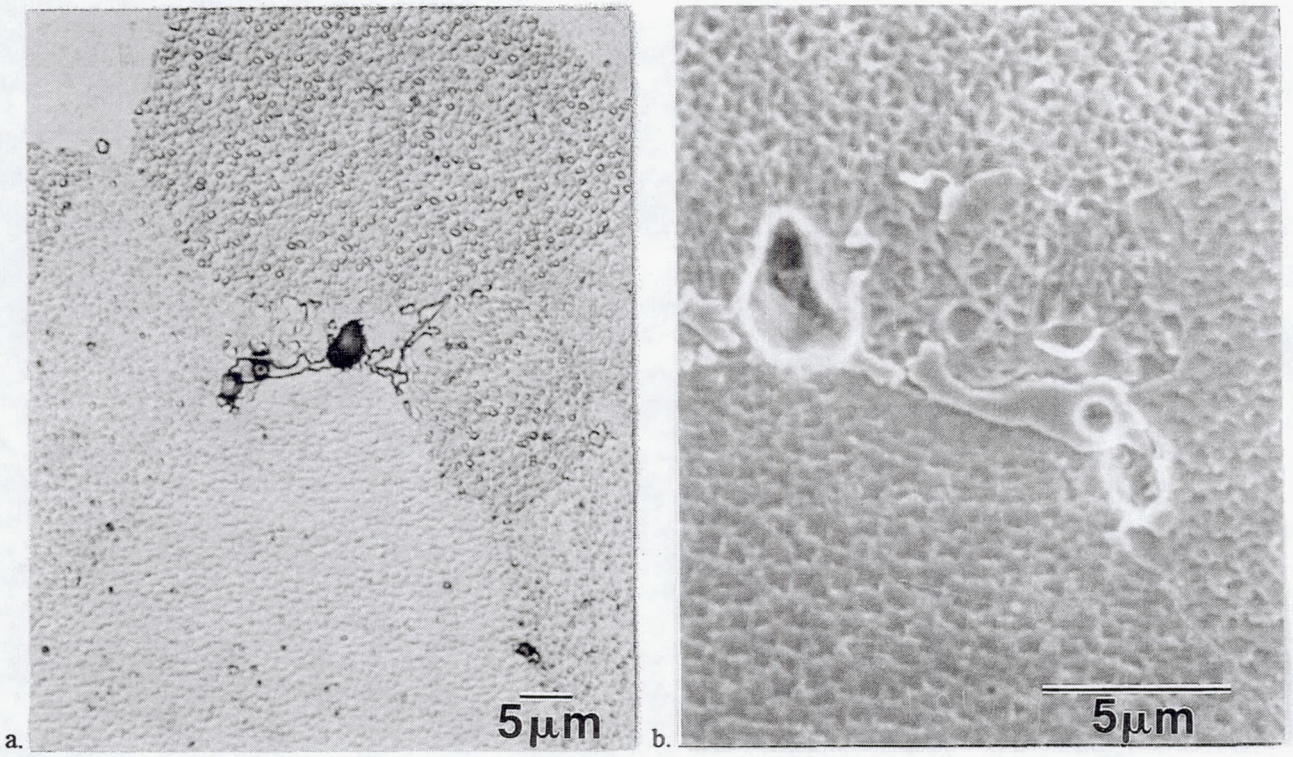

Fig. 10. Micrographs of $(Mo,Cr)_3B_2$ boride and large Type B pore in high boron KM4: a. optical micrograph of boride, b. SEM micrograph of boride, c. optical micrograph of large Type B pore.

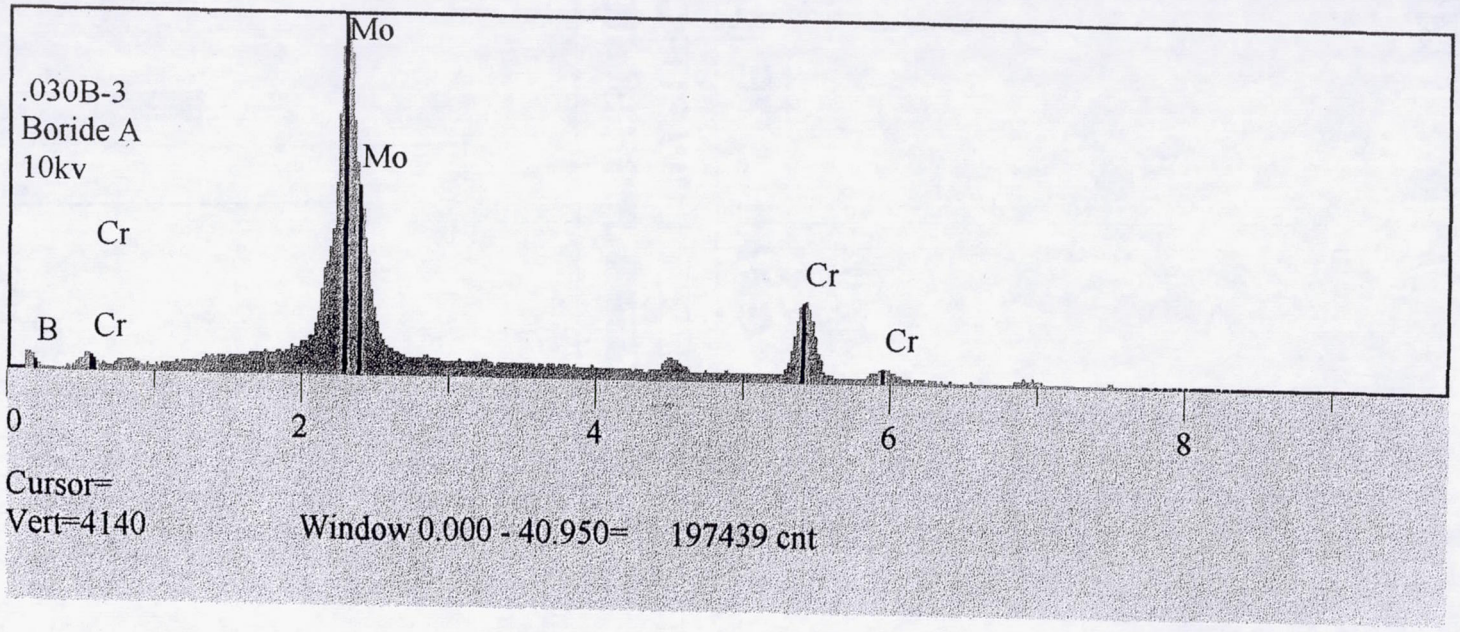

Fig. 11. Energy dispersive x-ray spectrum of $(Mo,Cr)_3B_2$ boride in high boron KM4.

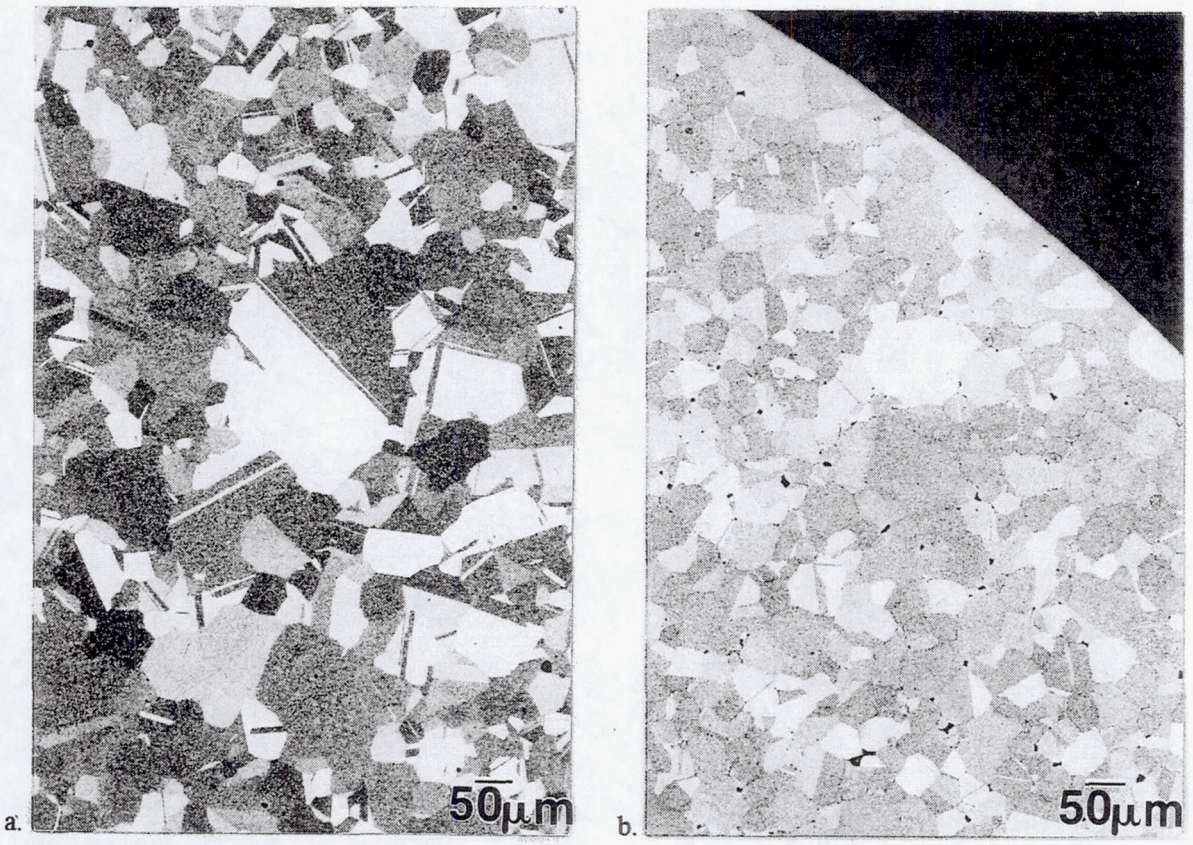

Fig. 12. Optical micrographs showing largest grains in typical specimens: a. low boron KM4, b. high boron KM4.

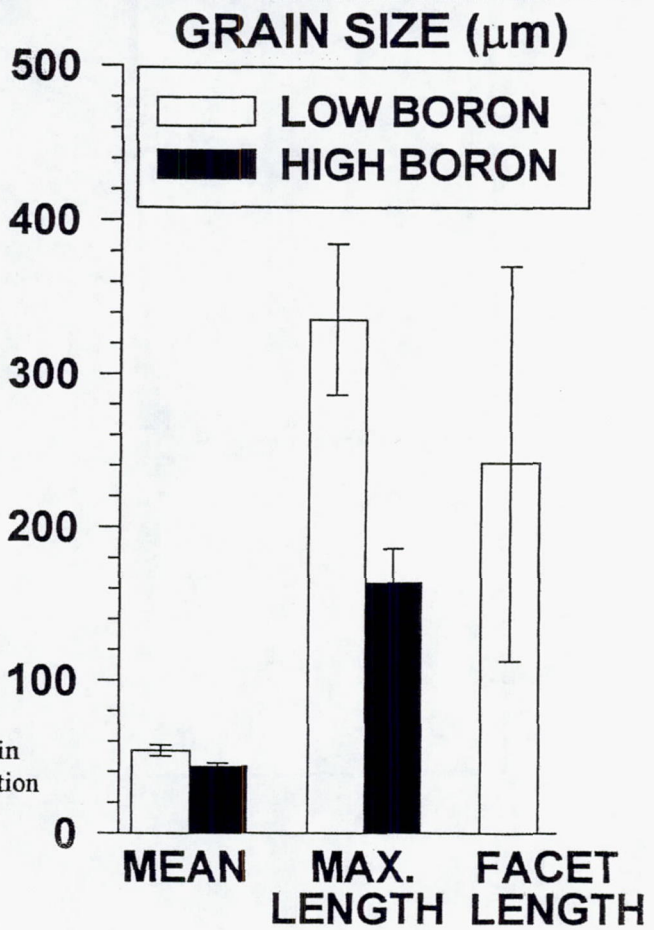

Fig. 13. Comparison of mean and maximum grain size for all specimen sections and at failure initiation sites, error bars indicate ±1 standard deviation.

a.

b.

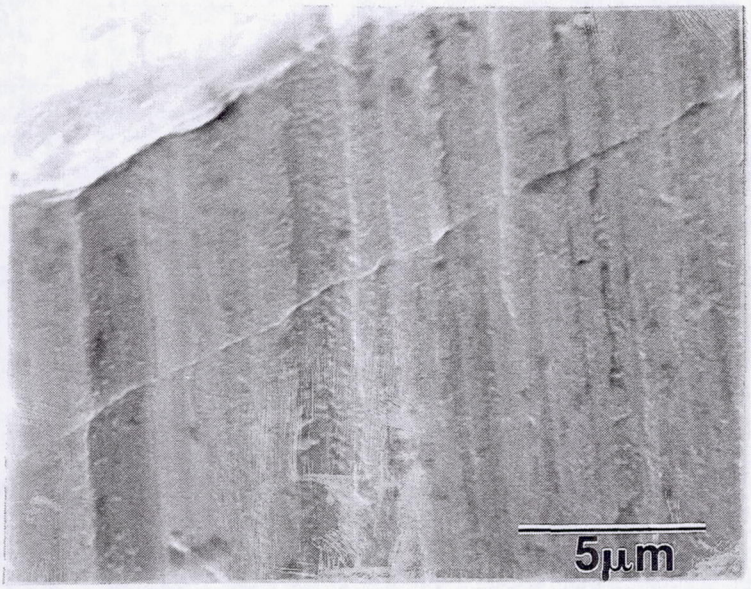

Fig. 14. SEM micrographs of the machined side adjoining a grain facet which initiated failure of a low boron KM4 specimen: a. secondary electron image, b. backscattered electron image.

REPORT DOCUMENTATION PAGE

Form Approved
OMB No. 0704-0188

1. AGENCY USE ONLY (*Leave blank*)	2. REPORT DATE	3. REPORT TYPE AND DATES COVERED
	September 2000	Technical Memorandum

4. TITLE AND SUBTITLE

The Effect of Boron on the Low Cycle Fatigue Behavior of Disk Alloy KM4

5. FUNDING NUMBERS

WU–714–04–10–00

6. AUTHOR(S)

Timothy Gabb, John Gayda, and Joseph Sweeney

7. PERFORMING ORGANIZATION NAME(S) AND ADDRESS(ES)

National Aeronautics and Space Administration
John H. Glenn Research Center at Lewis Field
Cleveland, Ohio 44135–3191

8. PERFORMING ORGANIZATION REPORT NUMBER

E–12454

9. SPONSORING/MONITORING AGENCY NAME(S) AND ADDRESS(ES)

National Aeronautics and Space Administration
Washington, DC 20546–0001

10. SPONSORING/MONITORING AGENCY REPORT NUMBER

NASA TM—2000-210458

11. SUPPLEMENTARY NOTES

Timothy Gabb and John Gayda, NASA Glenn Research Center; and Joseph Sweeney, Gilcrest Electric and Supply Company, 3000 Aerospace Parkway, Brook Park, Ohio 44142. Responsible person, Timothy Gabb, organization code 5120, (216) 433–3272.

12a. DISTRIBUTION/AVAILABILITY STATEMENT

Unclassified - Unlimited
Subject Category: 26 Distribution: Nonstandard

This publication is available from the NASA Center for AeroSpace Information, (301) 621–0390.

12b. DISTRIBUTION CODE

13. ABSTRACT ***(Maximum 200 words)***

The durability of powder metallurgy nickel base superalloys employed as compressor and turbine disks is often limited by low cycle fatigue (LCF) crack initiation and crack growth from highly stressed surface locations (corners, holes, etc.). Crack growth induced by dwells at high stresses during aerospace engine operation can be particularly severe. Supersolvus solution heat treatments can be used to produce coarse grain sizes approaching ASTM 6 for improved resistance to dwell fatigue crack growth. However, the coarse grain sizes reduce yield strength, which can lower LCF initiation life. These high temperature heat treatments also can encourage pores to form. In the advanced General Electric disk superalloy KM4, such pores can initiate fatigue cracks that limit LCF initiation life. Hot isostatic pressing (HIP) during the supersolvus solution heat treatment has been shown to improve LCF initiation life in KM4, as the HIP pressure minimizes formation of the pores. Reduction of boron levels in KM4 has also been shown to increase LCF initiation life after a conventional supersolvus heat treatment, again possibly due to effects on the formation tendencies of these pores. However, the effects of reduced boron levels on microstructure, pore characteristics, and LCF failure modes in KM4 still need to be fully quantified. The objective of this study was to determine the effect of boron level on the microstructure, porosity, LCF behavior, and failure modes of supersolvus heat treated KM4.

14. SUBJECT TERMS

Superalloy; Inclusions; Porosity; Fatigue

15. NUMBER OF PAGES

25

16. PRICE CODE

A03

17. SECURITY CLASSIFICATION OF REPORT	18. SECURITY CLASSIFICATION OF THIS PAGE	19. SECURITY CLASSIFICATION OF ABSTRACT	20. LIMITATION OF ABSTRACT
Unclassified	Unclassified	Unclassified	